Dual channel optical detector for trace water chemodosimetry and imaging of live cells†

Guangwen Men,[a] Guirong Zhang,[b] Chunshuang Liang,[a] Huiling Liu,[a] Bing Yang,[a] Yuyu Pan,[a] Zhenyu Wang,[b] Shimei Jiang[a]*

(Electronic Supplementary Information)

[a]State Key Laboratory of Supramolecular Structure and Materials, Jilin University, 2699 Qianjin Avenue, Changchun 130012, P. R. China.E-mail: smjiang@jlu.edu.cn

Tel: +86-431-85168474 Fax: +86-431-85193421

[b]College of Life Science, Jilin University, 2699 Qianjin Avenue, Changchun, 130012, P. R. China.

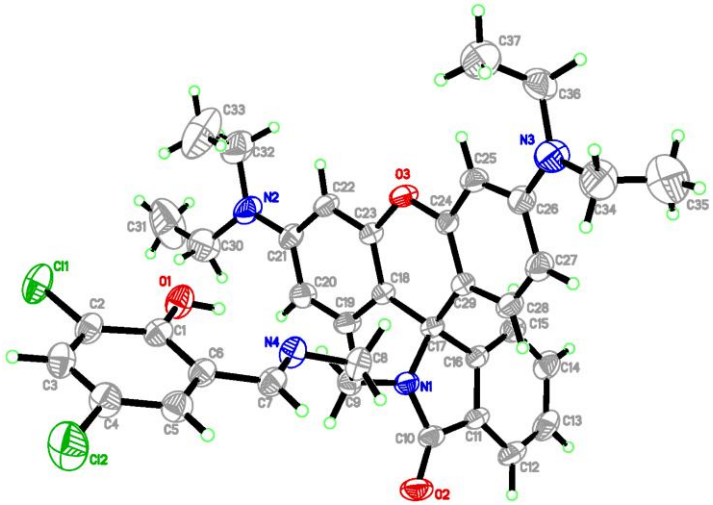

Fig. S1 ORTEP diagram of the compound **1** (30% probability factor for the thermal ellipsoids).

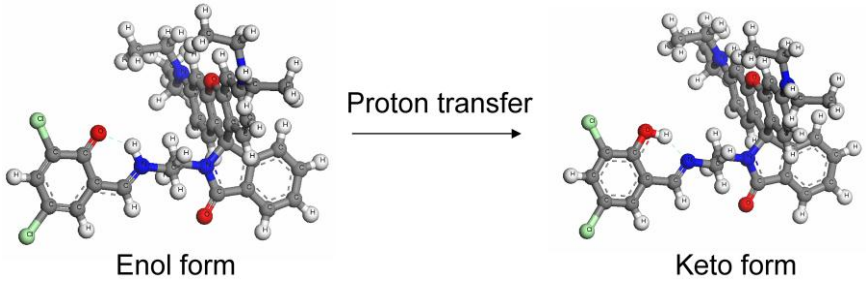

Scheme S1. DFT optimized geometries of enol and keto tautomeric form of **1**.

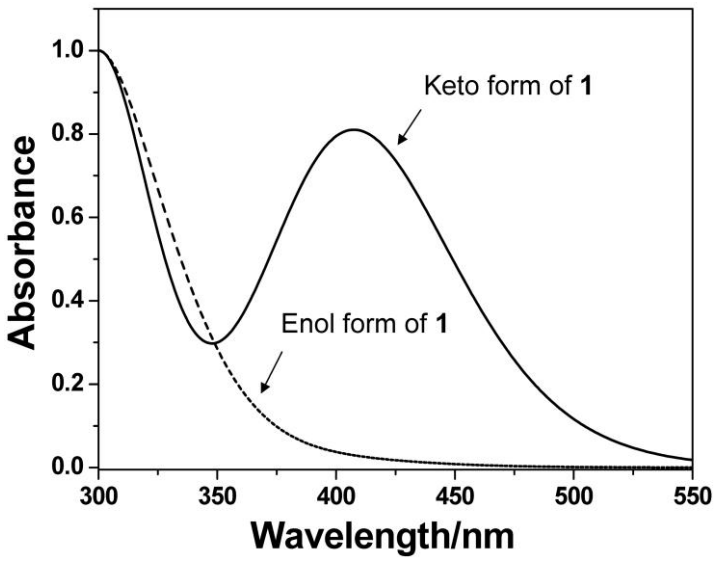

Fig. S2 Calculated absorption spectra of enol and keto structure of **1** in gas phase by TD/DFT method (normalized).

Table S1. Thermodynamic Characteristics of Proton Transfer Equilibrium (from UV-Vis Spectra) of **1** at 293 K.

Compound	4		5		6[b]		7		8		9[b]	
	K_{PT}[a]	ΔG^0_{PT} kJ/mol	K_{PT}	ΔG^0_{PT} kJ/mol	K_{PT}	ΔG^0_{PT} kJ/mol	K_{PT}	ΔG^0_{PT} kJ/mol	K_{PT}	ΔG^0_{PT} kJ/mol	K_{PT}	ΔG^0_{PT} kJ/mol
n-hexane	0.0088	11.52	0.0047	13.04	0.0167	9.97	0.0016	15.73	0.0273	8.77	0.0065	12.27
toluene	0.0654	6.64	0.0380	7.96	0.0150	10.23	0.0132	10.54	0.0169	9.93	0.0102	11.18
THF	0.1792	4.19	0.1010	5.58	0.0194	9.61	0.0116	10.86	0.0216	9.34	0.0071	12.06
ethyl acetate	0.2198	3.69	0.1043	5.51	0.0272	8.78	0.0048	12.98	0.0267	8.23	0.0066	12.25
chloroform	0.2812	3.09	0.2210	3.68	0.0346	8.19	0.0128	10.62	0.0481	7.39	0.0181	9.77
acetonitrile	0.8430	0.42	0.3596	2.49	0.0361	8.09	0.0414	7.76	0.0208	9.44	0.0085	11.61
methanol	2.4847	-2.22	1.3217	-0.68	0.128	5.01	0.3807	2.35	0.1643	4.4	0.0207	9.44

[a] Proton transfer equilibrium constants defined as $K_{PT} = A_{keto} / A_{enol}$ (ratio of the keto absorbance at around 430 nm for compound **4**-**6** and around 410 nm for compound **7**-**9** to the enol absorbance at around 338 nm for compound **4**-**6** and around 320 nm for compound **7**-**9**). [b] Due to strongly overlapping bands, these values are only approximate.

Proton transfer equilibrium constants defined as $K_{PT} = A_{keto} / A_{enol}$ and free standard energy change ΔG^0_{PT} of compounds **4**-**9** are listed in **Table S1** at 293 K[11a, 11e]. It should be noted that the absolute values of the thermodynamic characteristics of the proton transfer process in compounds **7**-**9** are much lower than in compounds **4**-**6**. A probable explanation is that the substitution of 1- and 3-position chlorine atoms coupled to the phenol group leads to the increase in acidity of the phenolic part of compounds **4**-**6**. Thus for compounds **4**-**6**, one observes a stronger equilibrium shift in the direction of proton transfer forms than in compounds **7**-**9**. On the other hand, we also found the K_{PT} values of compounds **4**-**6** show a clear increase in the order **6**＜**5**＜**4** in the same solvent from **Table S1**, indicating that the increase of molecular steric repulsion blocks the process of proton transfer, which can be explained by an increase of steric shielding of the acid-base center from the active solvent molecules[11a].

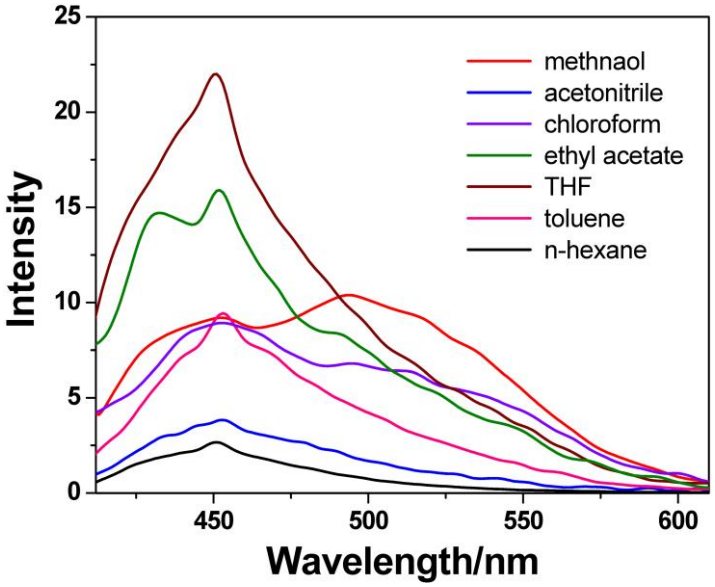

Fig. S3 Fluorescence spectra of **1** in different organic solvents. Excitation was at 400 nm.

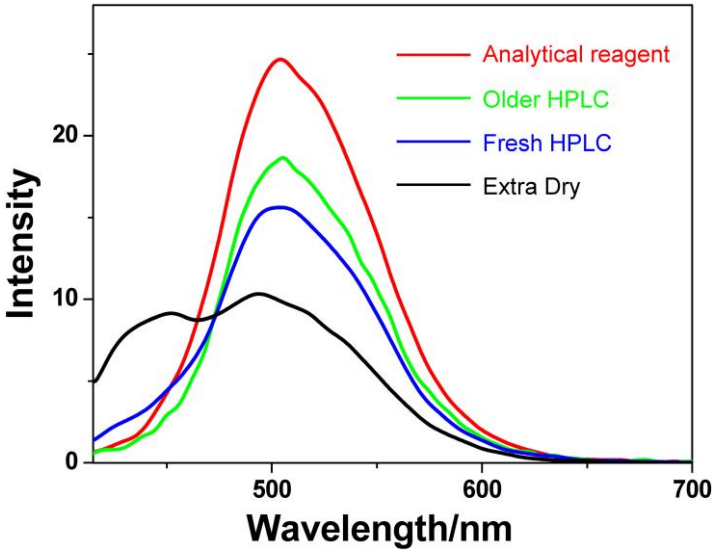

Fig. S4 Fluorescence spectra of **1** in various grades of commercial methanol. (λ_{ex} = 400 nm, [**1**] = 50 μM).

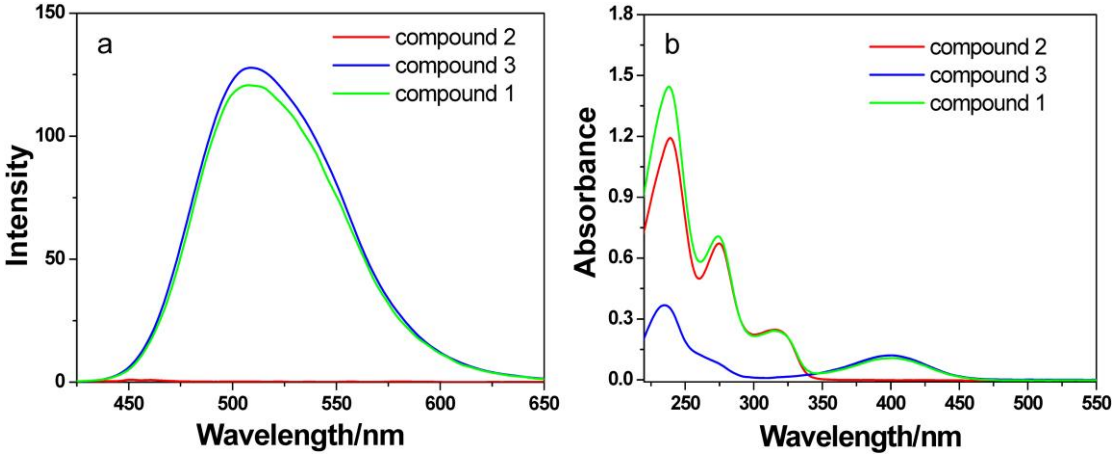

Fig. S5 (a) Fluorescence and (b) absorption spectra of 20 μM of **1**, **2** and **3** in methanol-H_2O (1 : 1, v/v, pH = 7.0) solution, respectively.

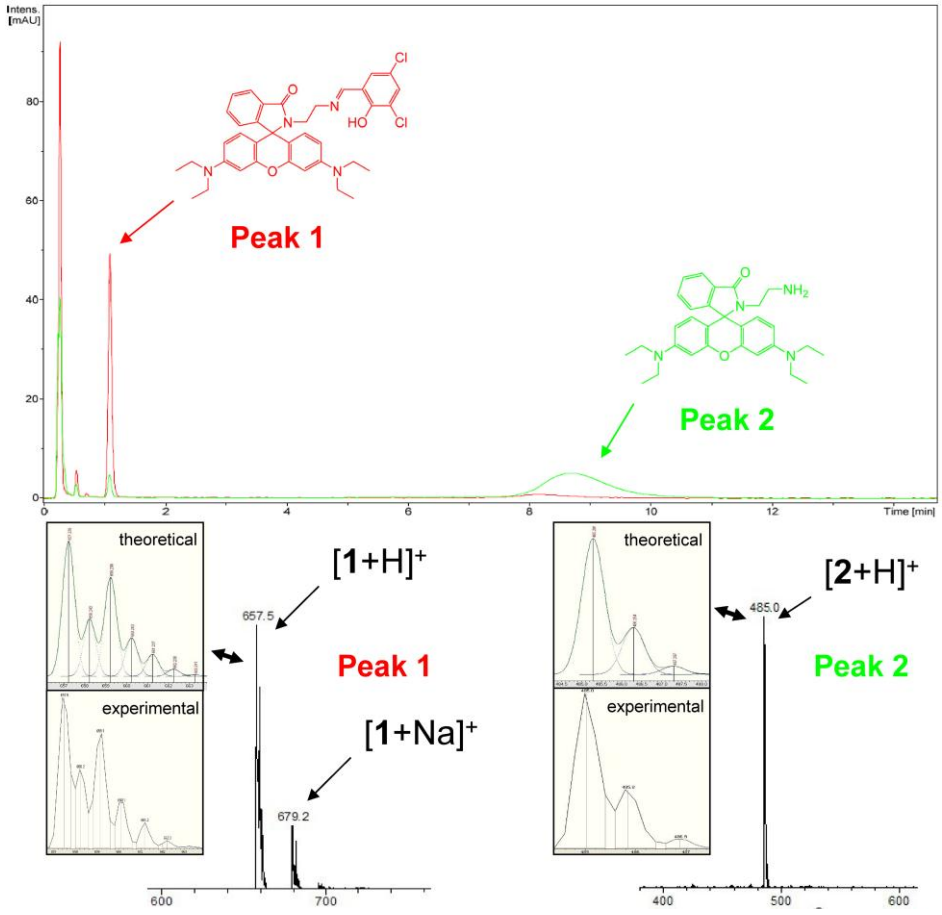

Fig. S6 LCMS analysis of 20 μM of **1** in methanol-H_2O (1 : 1, v/v) after (red line) 1 min and (green line) 2 h, proving the existence of the hydrolysis process. (UV detection at 274 nm).

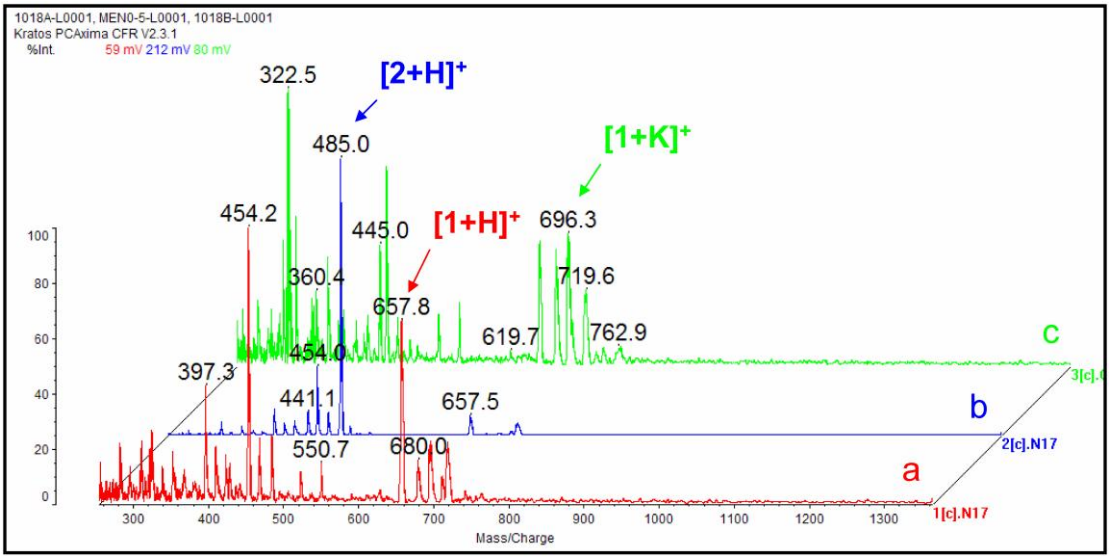

Fig. S7 MALDI-TOF mass spectrum of 20 μM **1** in methanol-H_2O (1:1, v/v) after (a) 1 min and (b) 2 h. (c) MALDI-TOF mass spectrum of 20 μM **1** in methanol after 2 h.

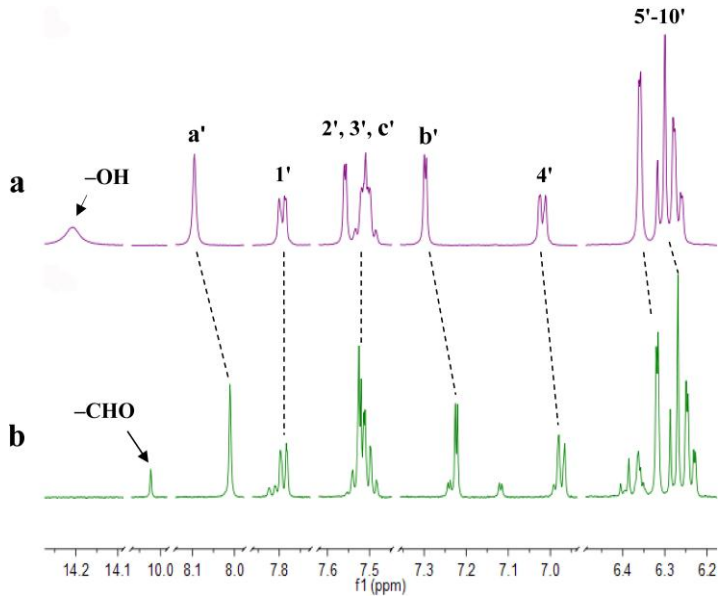

Fig. S8 ^{1}H NMR spectra of **1** in (a) DMSO-d_6 and (b) DMSO-d_6 containing 10% D_2O (in the aromatic range).

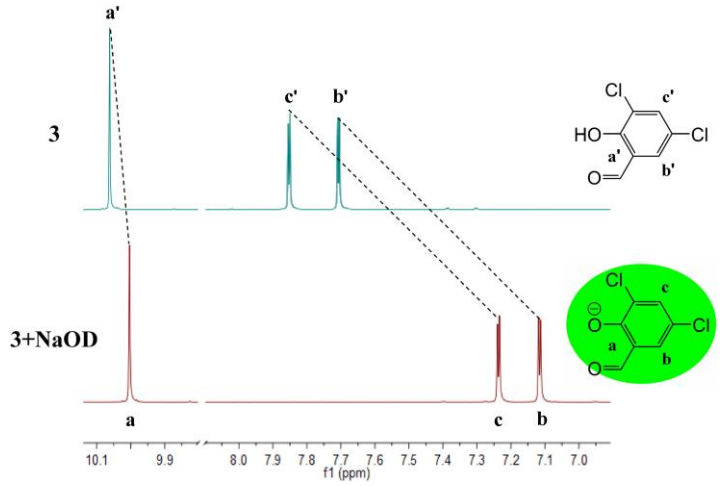

Fig. S9 ^{1}H NMR spectra of **3** and **3** + NaOD (*ca.* 1 equiv.) in DMSO-d_6 containing 10% D_2O.

3 was in its deprotonated form when it was in higher pH (in **3**+NaOD solution). Consequently, the deprotonation of the OH group brought electron density onto the 3-5-dicholori-subsituted aromatic framework, and the protons of the dicholori-subsituted aromaitic moiety and the aldehyde group distinctly shifted upfield. (as shown in **Fig. S9**)

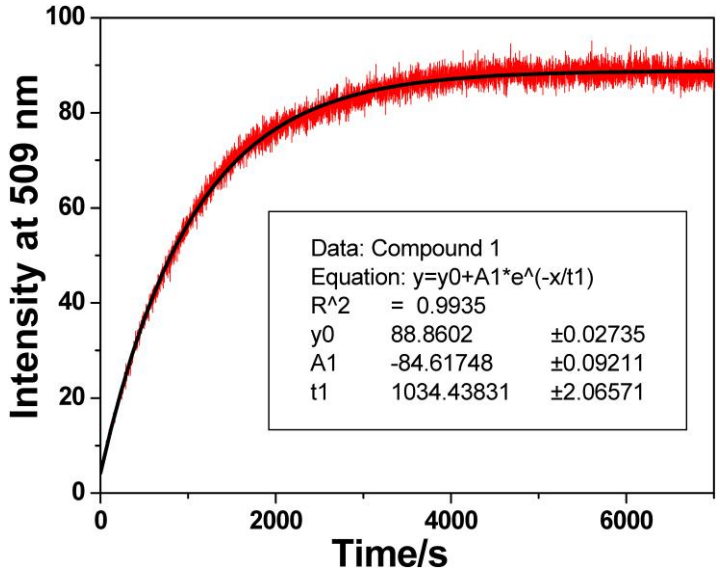

Fig. S10 (a) Time course of the fluorescence intensity at 509 nm of 20 μM **1** in methanol-H_2O (1:1, v/v) solution at room temperature. The box indicates kinetic analysis results based on first decay model.

Table S2. Speed constants (k) in methanol, THF and acetonitrile with different water contents at 55℃.

	water content (v/v)	speed constant (k)
MeOH	0.5%	0.00057
	3%	0.00153
	10%	0.00394
THF	10%	0.00206
	30%	0.00329
	50%	0.00594
CH_3CN	1%	0.00046
	5%	0.00119
	10%	0.00178

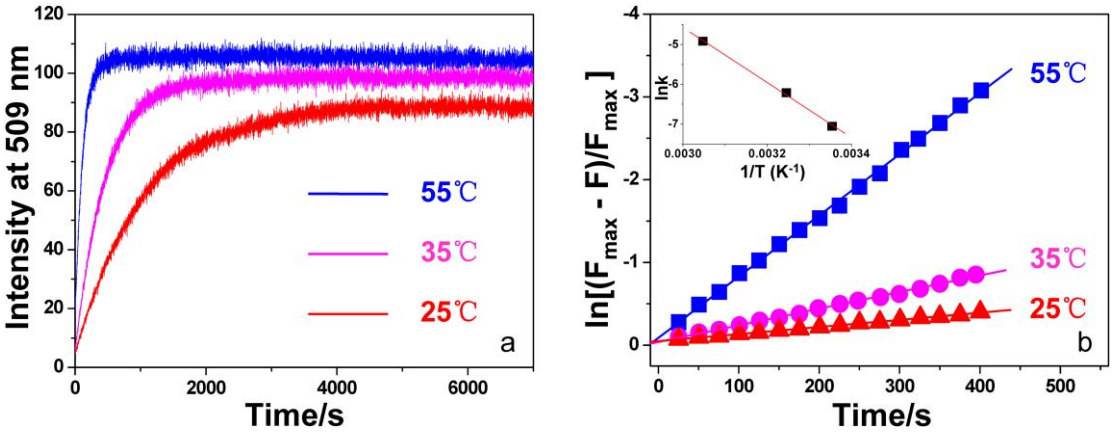

Fig. S11 (a) Time course of the fluorescence intensity at 509 nm of 20 μM **1** in methanol-H_2O (1:1, v/v) solution at different temperatures. (b) Curves fitted with one-order reaction dynamics { $\ln[(F_{max}-F_t)/F_{max}] = -kt$ } and speed constant (k) was calculated: k_{25c} = 0.00086 s^{-1} (T = 25℃), k_{35c} = 0.00200 s^{-1} (T = 35℃), k_{55c} = 0.00739 s^{-1} (T = 55℃). Conditions: [**1**] = 20 μM, ex/em = 400/508 nm, 50% (v/v) methanol-H_2O. Inset: Curves fitted with Arrhenius expressions (lnk = $-E_a/RT+\ln A$) and activation energy was calculated: E_a = 57.9 KJ/mol.

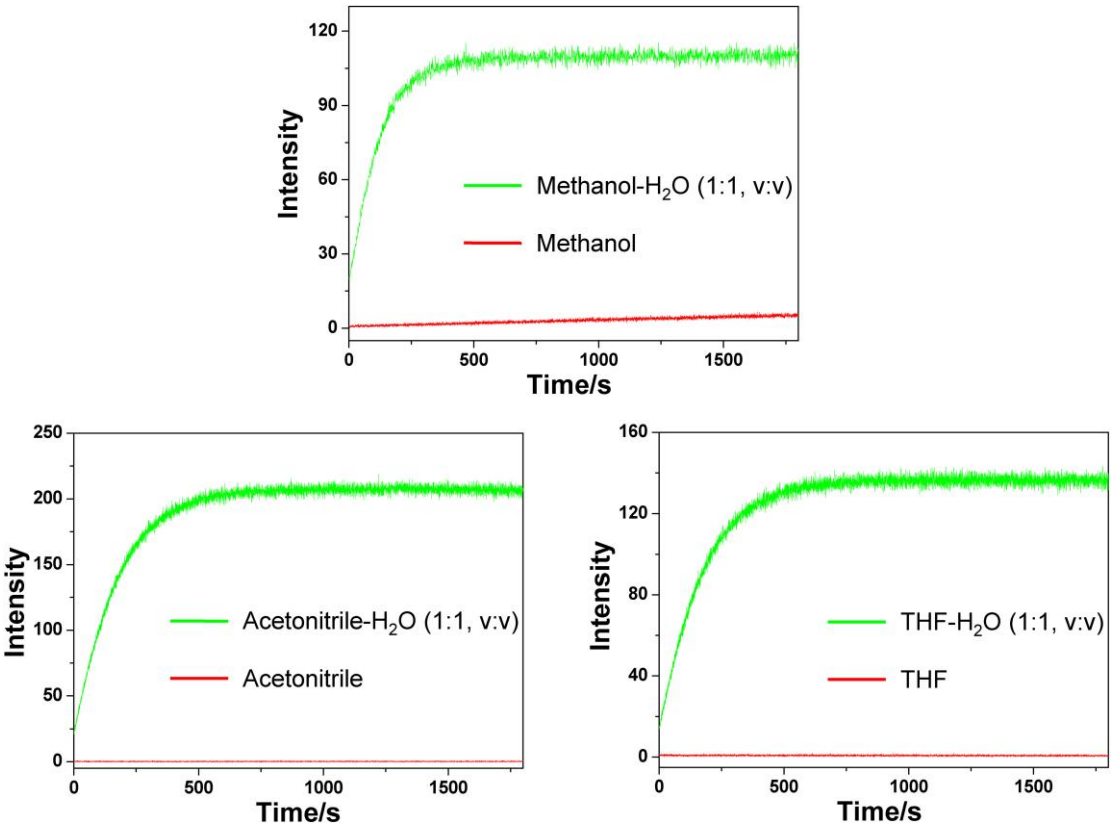

Fig. S12 Time course of the fluorescence intensity at 509 nm of 20 μM **1** in different organic solvent and its mixture solution with water under heating. Condition: ex/em = 400/509 nm, at 55℃.

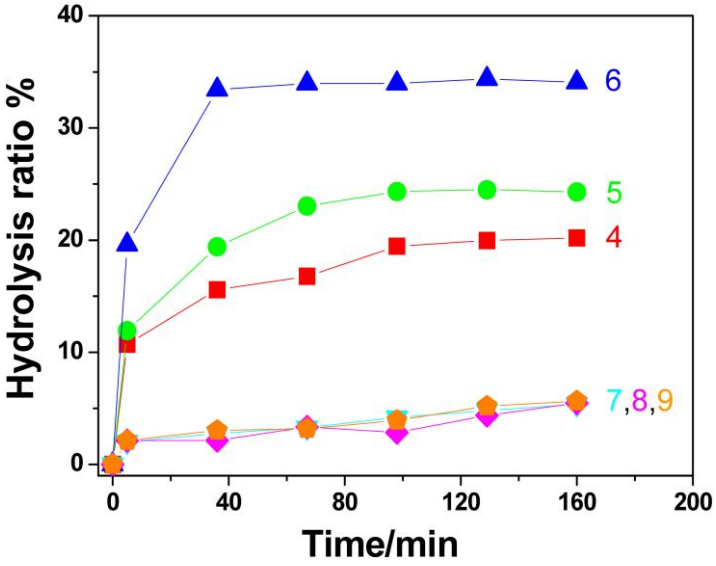

Fig. S13 Time course of hydrolysis ratios of compound **4**-**9** in DMSO-d_6/D_2O (9:1, v/v) solution, which was calculated from NMR speatra. The concentration of compound **4**-**9** is 6.3 mM.

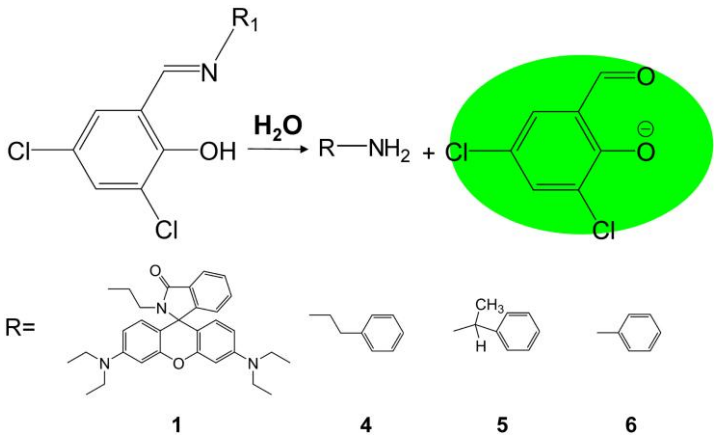

Scheme S2. Proposed water sensing mechanisms of **1**, **4**, **5** and **6**.

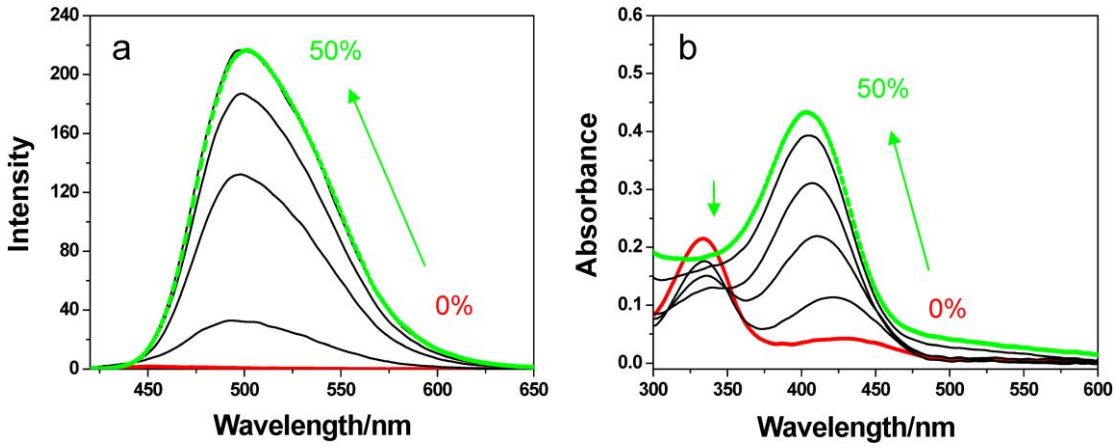

Fig. S14 Changes in the (a) fluorescence and (b) spectra of **4** with increasing water (0-50% v/v) in THF. (λ_{ex} = 400 nm, [**4**] = 20 μM)

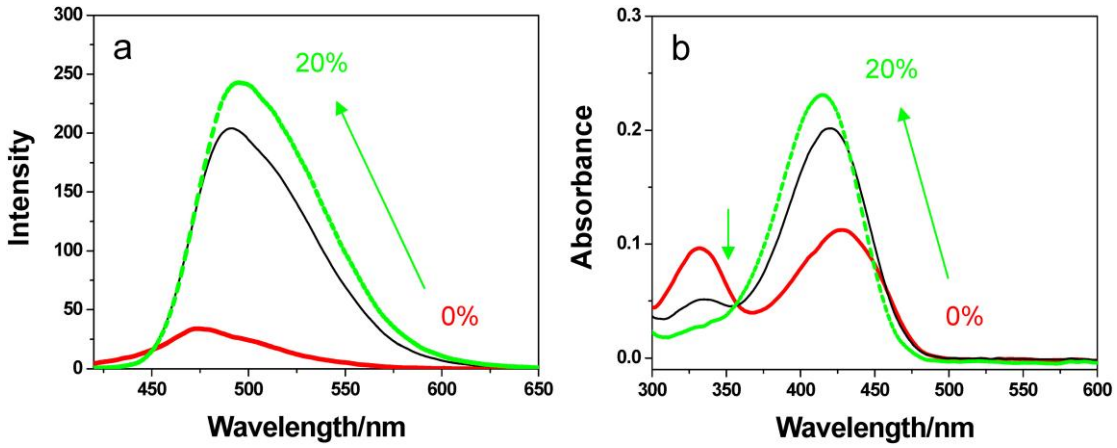

Fig. S15 Changes in the (a) fluorescence and (b) spectra of **4** with increasing water (0-20% v/v) in DMF. (λ_{ex} = 400 nm, [**4**] = 20 μM)

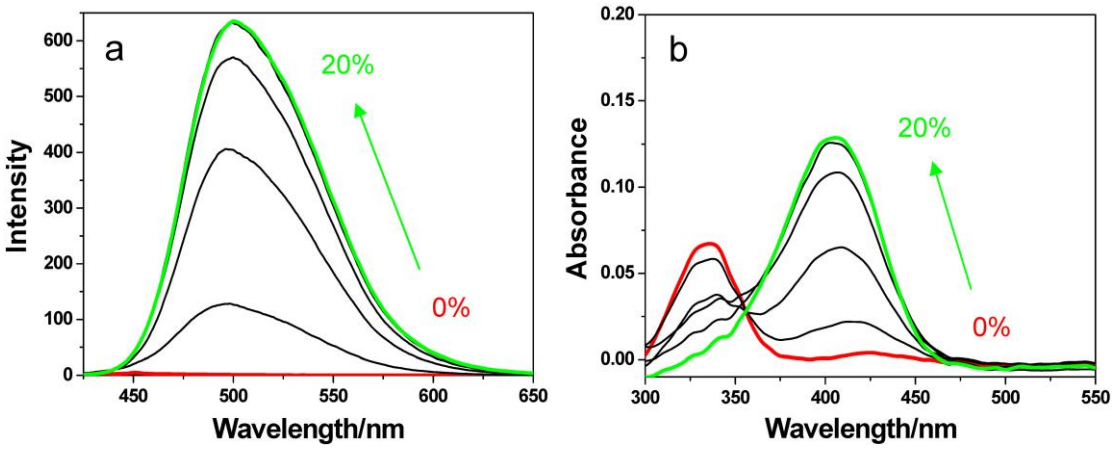

Fig. S16 Changes in the (a) fluorescence and (b) spectra of **5** with increasing water (0-20% v/v) in THF. (λ_{ex} = 400 nm, [**5**] = 20 μM)

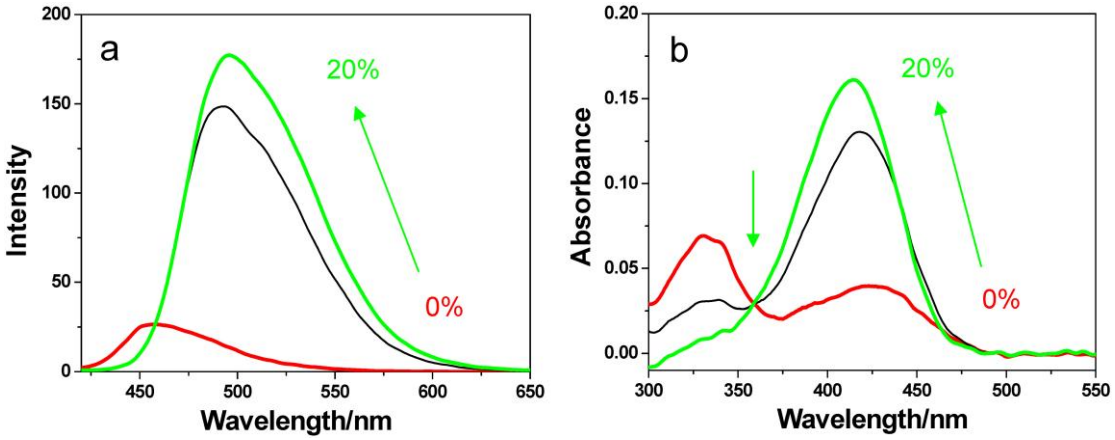

Fig. S17 Changes in the (a) fluorescence and (b) absorption spectra of **5** with increasing water (0-20% v/v) in DMF. (λ_{ex} = 400 nm, [**5**] = 20 μM)

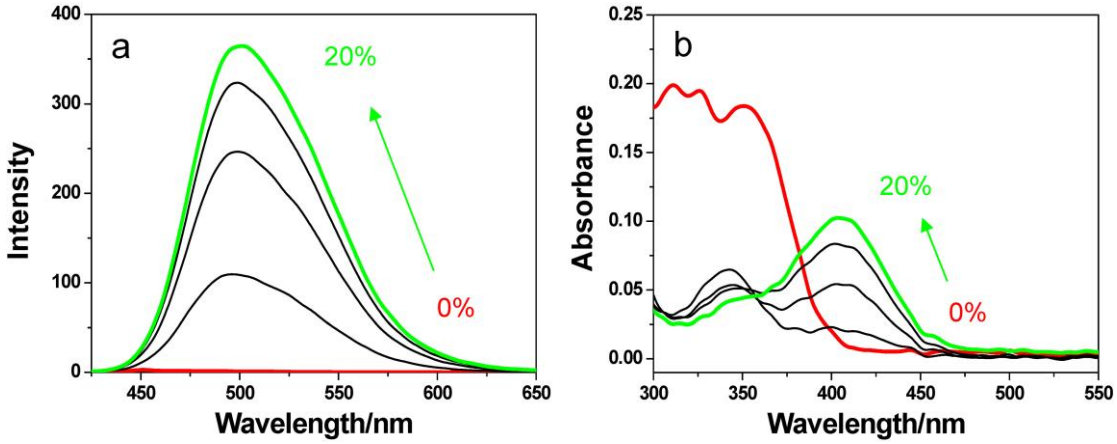

Fig. S18 Changes in the (a) fluorescence and (b) absorption spectra of **6** with increasing water (0-20% v/v) in THF. (λ_{ex} = 400 nm, [**6**] = 20 μM)

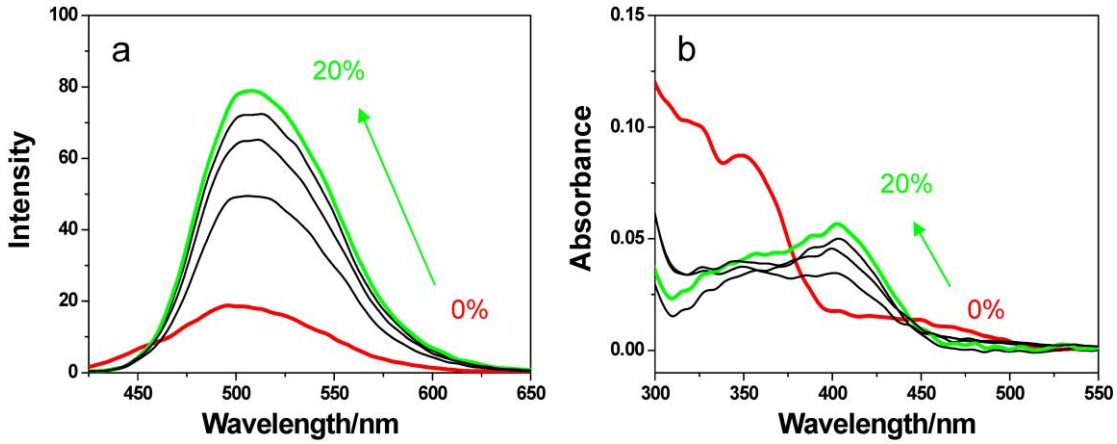

Fig. S19 Changes in the (a) fluorescence and (b) absorption spectra of **6** with increasing water (0-20% v/v) in methanol. (λ_{ex} = 400 nm, [**6**] = 20 μM)

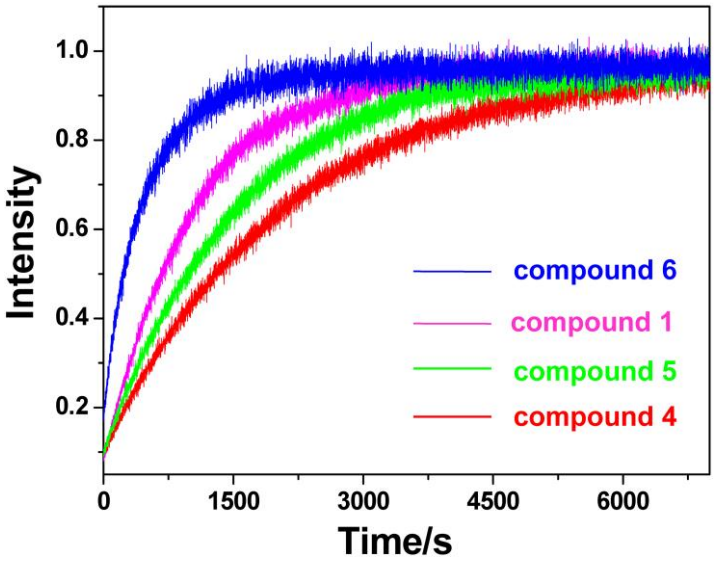

Fig. S20 (a) Time course of the fluorescence intensity at 509 nm of 20 μM **1**, **4**, **5** and **6** in methanol-H_2O (1:1, v/v) solution at 25℃ (normalized). Curves fitted with one-order reaction dynamics { $\ln[(F_{max}-F_t)/F_{max}] = -kt$ } and speed constant (k) was calculated: $k_1 = 0.00086\ s^{-1}$ (compound **1**), $k_4 = 0.00048\ s^{-1}$ (compound **4**), $k_5 = 0.00067\ s^{-1}$ (compound **5**) and $k_6 = 0.00189\ s^{-1}$ (compound **6**). Conditions: ex/em = 400/508 nm, 50% (v/v) methanol-H_2O, spectra was measured at 25℃.

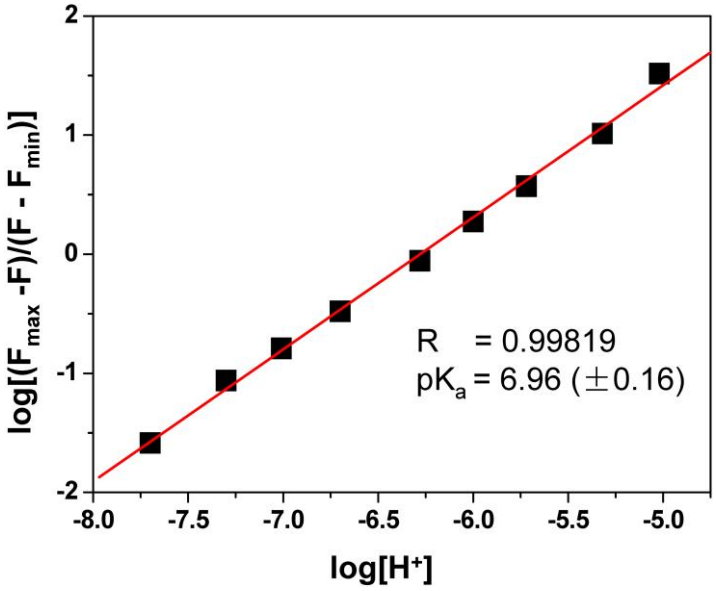

Fig. S21 Fluorescence intensity at 509 nm of **1** versus increasing concentration of $\log[H^+]$. The concentration of **1** was 20 μM.

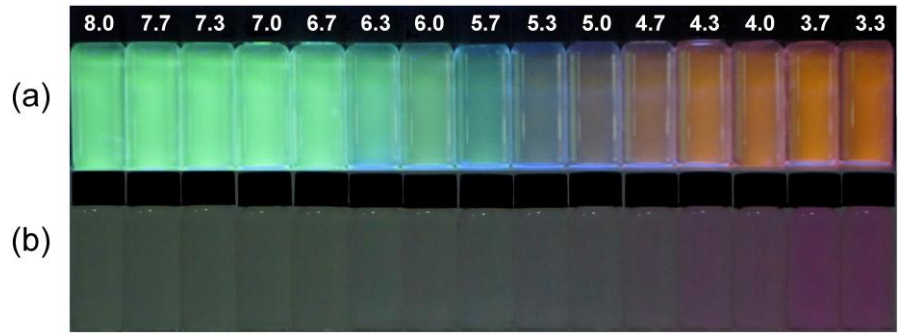

Fig. S22 (a) Fluorescence and (b) color changes of 20 μM of **1** in Britton-Robinson buffer solution (50% methanol cosolvent, 0.10 M NaCl) with different pH (3.3-8.0).

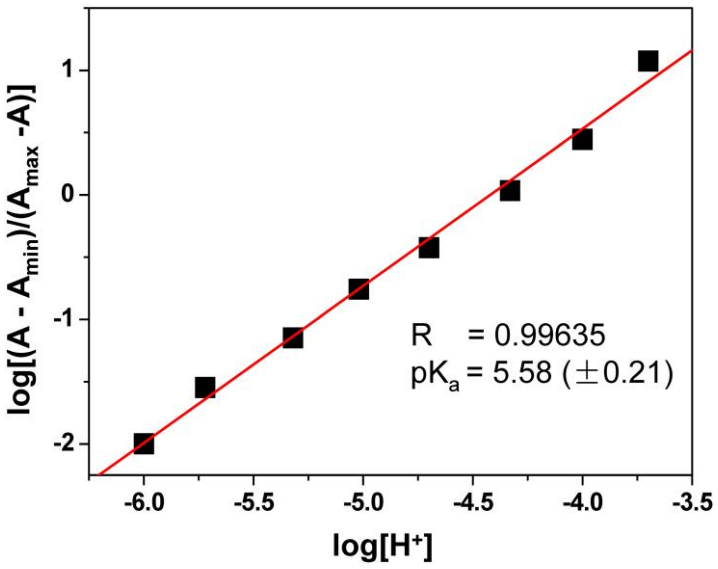

Fig. S23 Absorbance at 558 nm of **1** versus increasing concentration of log[H^+]. The concentration of **1** was 20 μM.

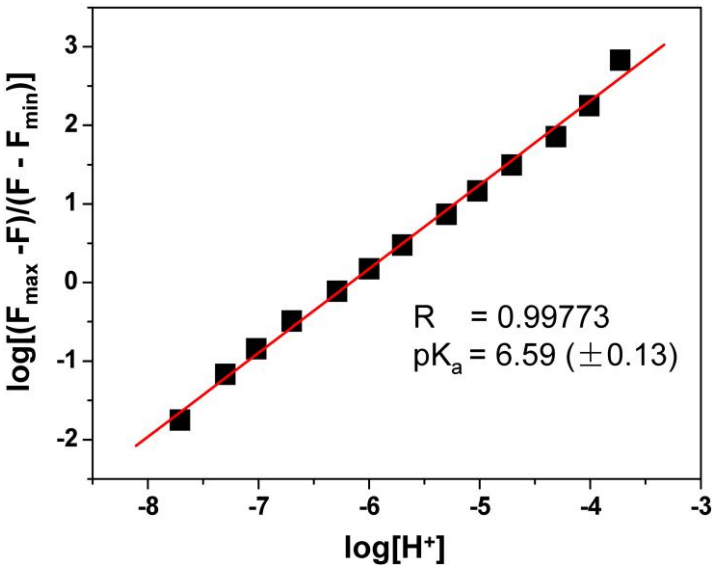

Fig. S24 Fluorescence intensity at 509 nm of **3** versus increasing concentration of log[H^+]. The concentration of **3** was 20 μM. The fluorescence response fits to a Hill coefficient of 1 (1.06861); It is consistent with the formation of a 1:1 stoichiometry for the **3** (phenoxide)-H^+ species.

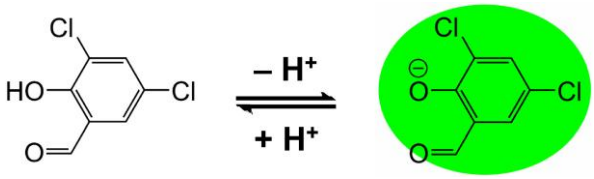

Scheme S3. pH-dependent equilibrium between the protonated and deprotonated forms of **3**.

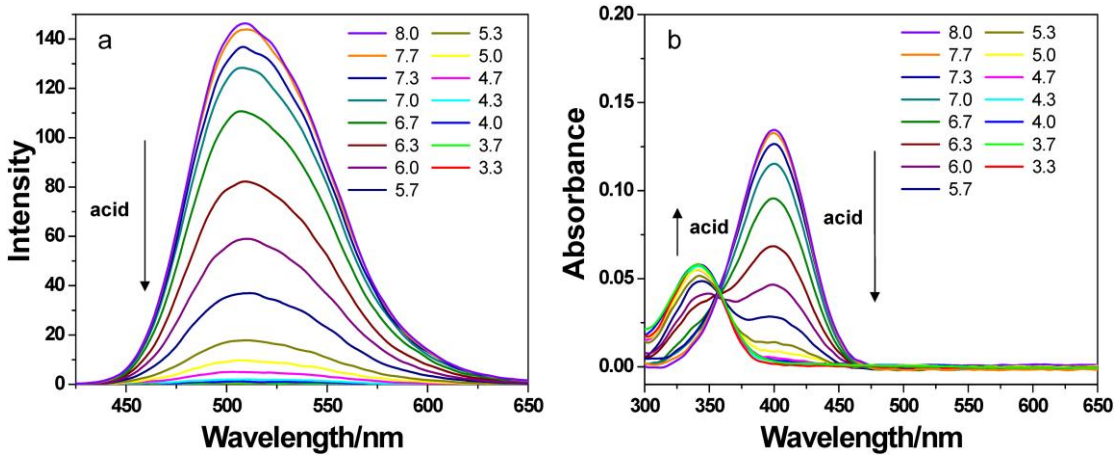

Fig. S25 (a) Fluorescence and (b) absorption spectra of 20 μM of **3** in Britton-Robinson buffer solution (50% methanol cosolvent, 0.10 M NaCl) with different pH (3.3-8.0).

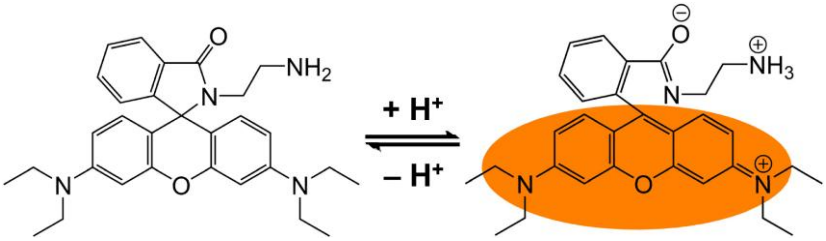

Scheme S4. pH-dependent equilibrium between the spirolactam and ring-opened forms of **2**.

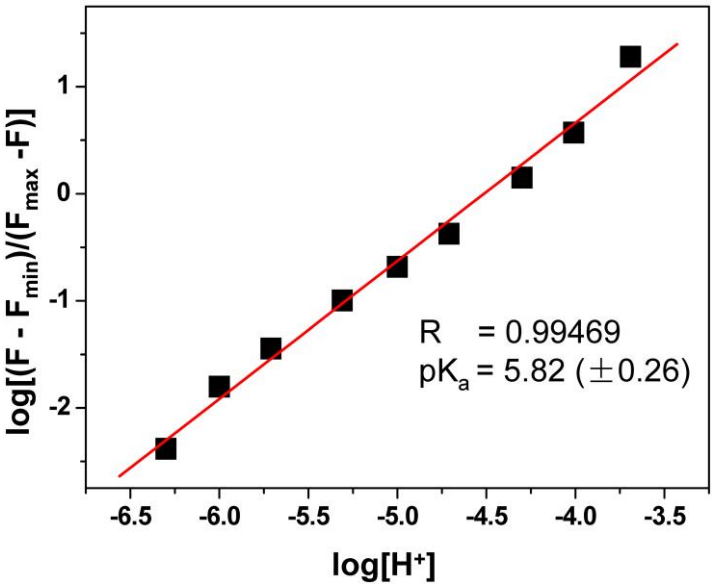

Fig. S26 Fluorescence intensity at 579 nm of **2** versus increasing concentration of log[H^+]. The concentration of **2** was 20 μM.

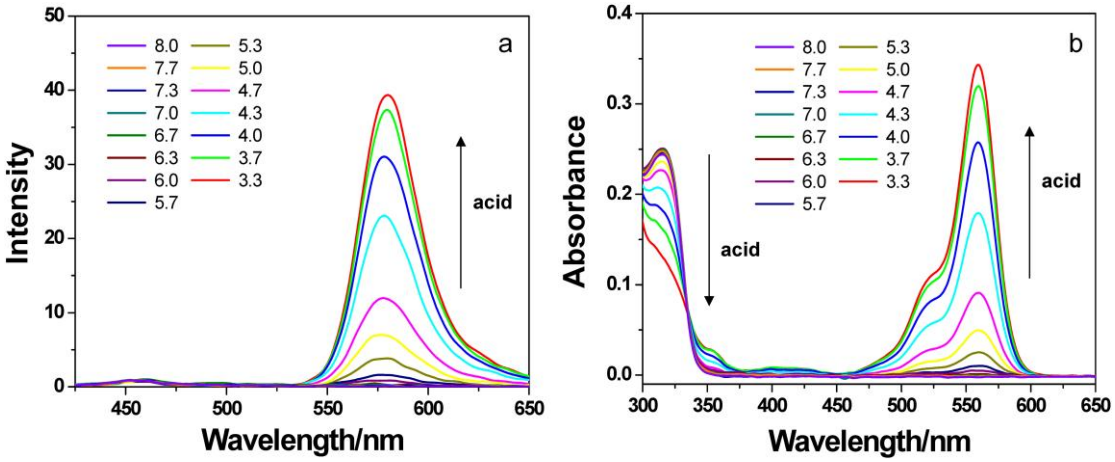

Fig. S27 (a) Fluorescence and (b) absorption spectra of 20 μM **2** in Britton-Robinson buffer solution (50% methanol cosolvent, 0.10 M NaCl) with different pH (3.3-8.0).

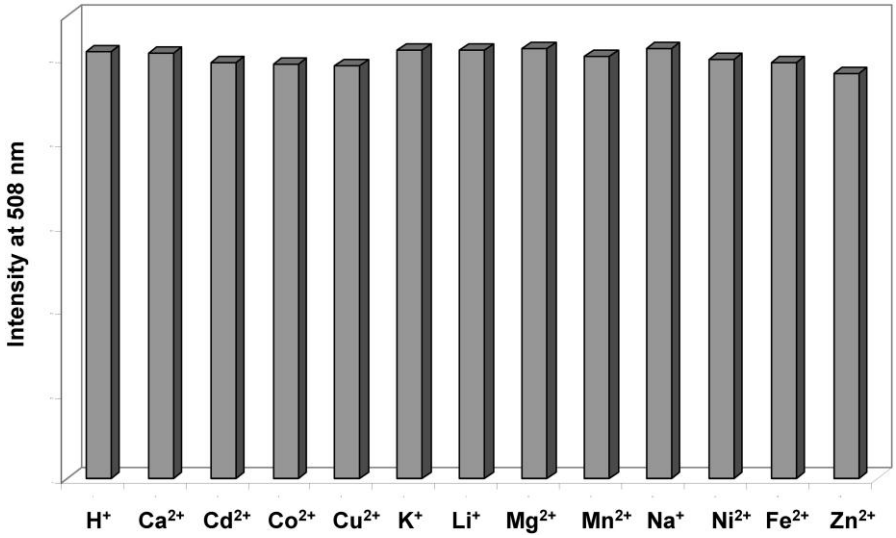

Fig. S28 The relative emission intensity (at 509 nm) change profile of **1** (20 μM) in the presence of various metal ions in Britton-Robinson buffer pH 7.0 (λ_{ex} = 400 nm). The final concentration of Li^+, Fe^{2+}, Mn^{2+}, Ni^{2+}, Co^{2+}, Cu^{2+}, Zn^{2+} and Cd^{2+} is 300 μM, respectively, while that of Na^+, K^+, Mg^{2+} and Ca^{2+} is 3 mM.

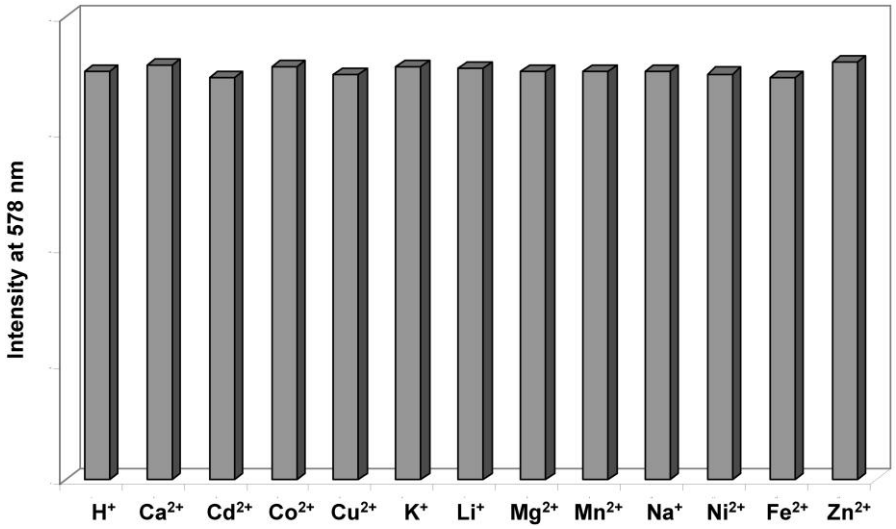

Fig. S29 The relative emission intensity (at 579 nm) change profile of **1** (20 μM) in the presence of various metal ions in Britton-Robinson buffer pH 3.0 (λ_{ex} = 400 nm). The final concentration of Li^+, Fe^{2+}, Mn^{2+}, Ni^{2+}, Co^{2+}, Cu^{2+}, Zn^{2+} and Cd^{2+} is 300 μM, respectively, while that of Na^+, K^+, Mg^{2+} and Ca^{2+} is 3 mM.

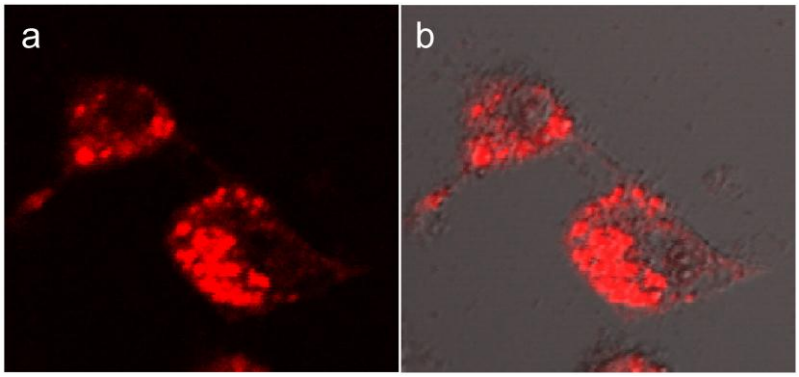

Fig. S30 Confocal fluorescence images of H^+ in HepG2 cells. (a) Fluorescence image of HepG2 cells treated with **1** (20 μM) for 24 h. (b) Combined images of phase contrast and fluorescence HepG2 cells incubated with **1** (λ_{ex} = 543 nm, shown in red, pH = 7.4).

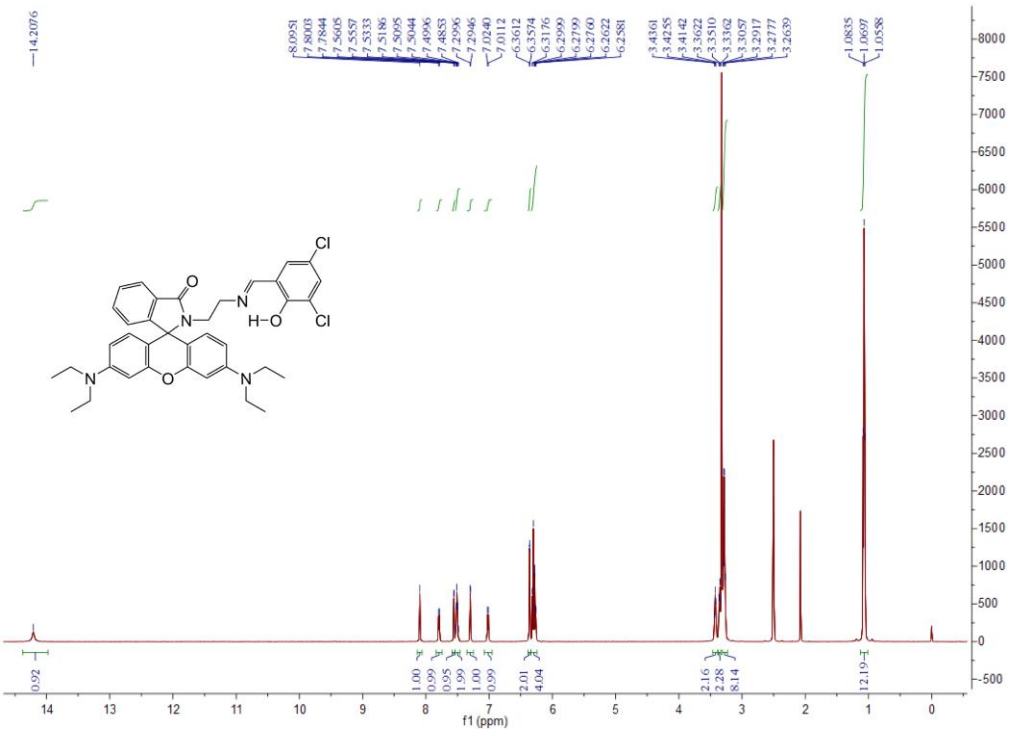

Fig. S31 ^{1}H NMR (DMSO-d_6, 500 MHZ) spectrum of **1**.

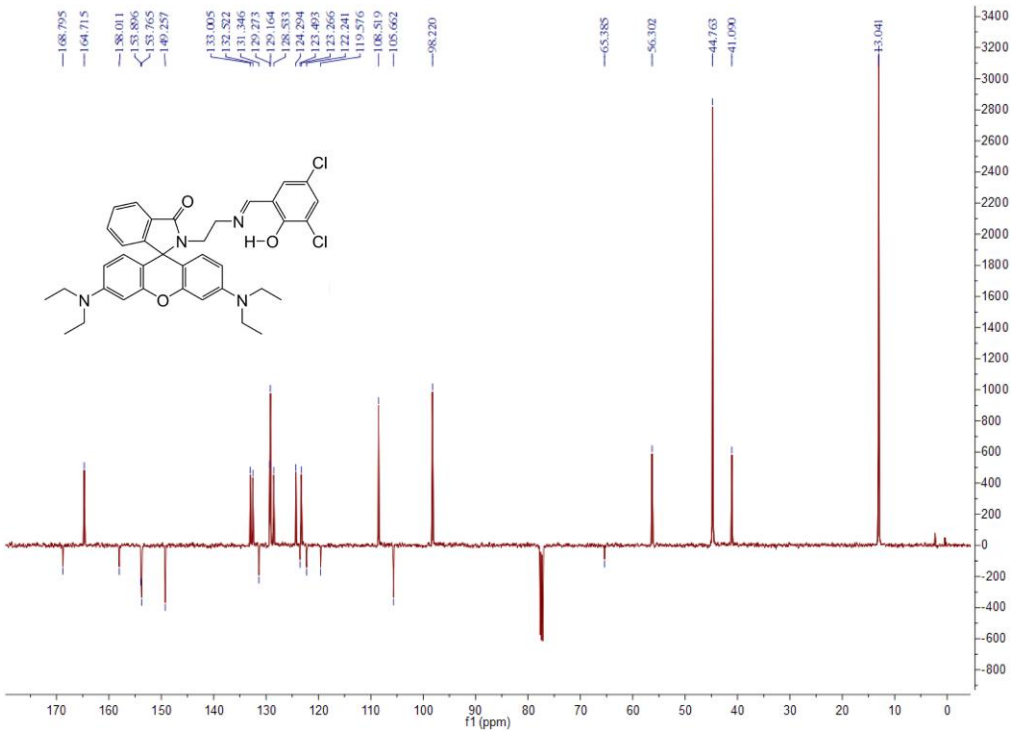

Fig. S32 DEPTQ ^{13}C NMR ($CDCl_3$, 500 MHZ) spectrum of **1**.

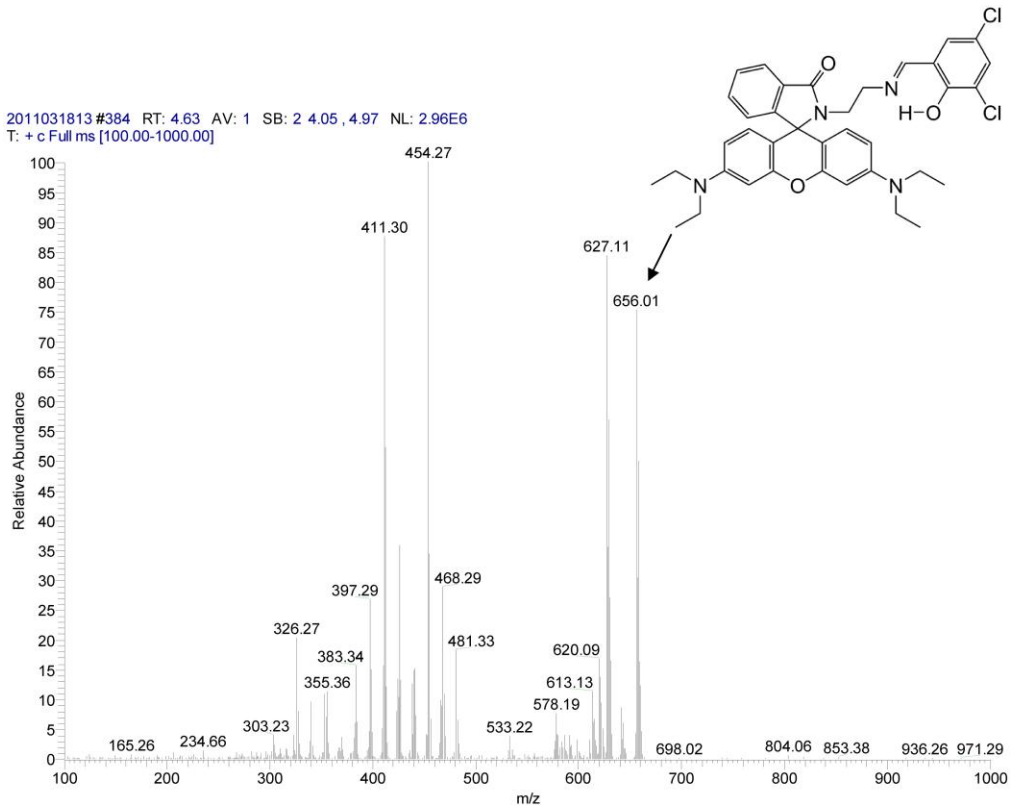

Fig. S33 Mass spectrum of **1**.

Table S4. Crystal data and structure refinement for **1**.

Identification code	**1**
Empirical formula	$C_{37}\,H_{38}\,Cl_2\,N_4\,O_3$
Formula weight	657.61
Temperature	293(2) K
Wavelength	0.71073 Å
Crystal system, space group	Monoclinic, P2(1)/c
Unit cell dimensions	a = 13.066(5) Å alpha = 90 deg. b = 9.757(3) Å beta = 116.000(17) deg. c = 29.525(11) Å gamma = 90 deg.
Volume	3383(2) Å^3
Z, Calculated density	4, 1.291 Mg/m^3
Absorption coefficient	0.234 mm^-1
F(000)	1384
Crystal size	0.45 x 0.42 x 0.17 mm
Theta range for data collection	3.02 to 27.48 deg.
Limiting indices	-16<=h<=16, -12<=k<=12, -38<=l<=38
Reflections collected / unique	30865 / 7746 [R(int) = 0.0521]
Completeness to theta = 27.48	99.8 %
Absorption correction	Semi-empirical from equivalents
Max. and min. transmission	0.9602 and 0.9027
Refinement method	Full-matrix least-squares on F^2
Data / restraints / parameters	7746 / 14 / 420
Goodness-of-fit on F^2	1.164
Final R indices [I>2sigma(I)]	R1 = 0.0632, wR2 = 0.1742
R indices (all data)	R1 = 0.1000, wR2 = 0.1917
Largest diff. peak and hole	0.458 and -0.309 e.Å^-3

Table S5. Hydrogen bonds for **1** [Å and deg.].

D-H...A	d(D-H)	d(H...A)	d(D...A)	<(DHA)
C(7)-H(7)...O(2)#1	0.93	2.34	3.241(3)	162.4
O(1)-H(1)...N(4)	0.82	1.82	2.549(3)	147.6